

RFSP-IST/CERBERUS SIMULATIONS WITH REACTOR REGULATING SYSTEM ON FOR CANDU 6 ACCIDENT ANALYSIS BY USING LARGER TIME-STEP SIZE

Dai-Hai Chung^{a*} and Cheon-Hwey Cho^b

Atomic Creative Technology Co., Ltd., Daejeon, Korea

*Corresponding author: dhchung@actbest.com

Abstract

The RFSP-IST/CERBERUS [1] simulations are conducted with RRS on in order to be applied for various accident analyses of CANDU 6 reactors, such as, LBLOCA, SBLOCA, In-CORE LOCA, LOR and moderator accidents. The steady-state initial conditions are set by coupling with the thermohydraulic code CATHENA [2], so that the initial conditions for the other important accident scenarios, e.g., LBLOCA, could also be established based upon the history of RRS actions that realistically follow the reactor operations. The representative cases studied here are selected in application to the moderator drain accidents, which demand the soundness and reliability of RRS predictions that show the capability of coping with the appreciable top-to-bottom flux tilts during the progress of transients. The CANDU 6 RRS algorithm requires a minimal time-step size of $\Delta t=0.5$ s that corresponds to the bulk control temporal sequences. An attempt has been made to double the time-step size to $\Delta t=1.0$ s. The results so obtained are compared against the simulation results that are obtained by using $\Delta t=0.5$ s.

1. Introduction

The beauty of the CANDU reactor design is the conceptual basis of the so-called time-average (TA) fuel burnup distribution in the core throughout the reactor's lifetime. Once the reactor core reaches equilibrium state after startup and initially loaded with fresh fuels, the design-based TA burnup distributions are maintained through daily on-power refuelling operations that are complemented by the Liquid Zone Controller (LZC) actions of the Reactor Regulating System (RRS). The prime and consistent CANDU 6 RRS actions using the LZCs consist of two parts: one is the bulk control for the global compensation of core system reactivity perturbations, which is accomplished by filling or draining the equal amounts of water into or from 14 zone controller compartments in unison for every 0.5 seconds, and the other is the spatial control which is performed every 2 seconds to fill or drain each zone controller compartments differentially in order to regulate zone power distributions in the core towards the target values based upon the TA design model.

The reactor physics computational tools, e.g., RFSP-IST [1] and SORO [3], then update the core fuel burnup distribution afterwards with normally 2~3 days interval to follow the reactor operations that have contributed to the fuel burnup progressions in time. This practice is based upon the static modelling of reactor core. In other words, the flux distribution in the core is calculated by importing

a: CTO, b: CEO

the snap-shot core configurations, such as, 14 zone controller levels and reactivity device positions, which represent the specific time-points in reactor operation history. Thus, the portion of fuel burnup progressions contributed by the actual RRS/LZC actions between any two consecutive and specific time-points are dismissed in these routine updates of fuel burnup distributions in the core that are based upon the practices of the static modelling of reactor core.

The fuel burnup distribution or the irradiation of each fuel bundle in the core are bound with certain errors coming from definite sources due to the mathematical and physical modelling deficiencies of the computer codes used. Firstly, the most basic error source would be the finite-differencing numerical scheme used to solve the neutron diffusion equations [1]. Secondly, the systematic error could be accounted for due to the deficiencies in modelling the reactivity devices and structural materials that are present in the reactor [4,5]. Thirdly, the fuel tables that are generated by using lattice codes, e.g., WIMS-IST and WIMS Utilities [6,7], also contribute to the fuel burnup error, which can be identified as flux-time dependent in contrast to the previous flux-space dependent systematic errors. The flux-time errors are directly related to the fuel burnup progressions in time, which are also directly depending on the way the burnup progressions are updated. Thus, any departure from the real time following of burnup progression contributes to the increase of fuel irradiation errors, which in turn become the source of wide-spread and accumulating errors in the flux solutions.

However, the effect of fuel burnup errors in steady-state simulations is not apparent due to the continuous replacement of the large burnup error bound old fuel bundles with fresh fuels, which are perfectly free of errors through the bi-directional on-power refuelling scheme of CANDU reactor system. Furthermore, the single and most important and practical observed quantity for the daily fuel management purposes at site would be the bundle or channel power, which is a spatially integrated quantity yielded with the some cancellation effects of fuel burnup errors to certain extent. Thus, the true effects of fuel burnup errors would not be fully revealed for the simulations that are needed to cope with the daily normal steady-state reactor operations.

The eminent effect of the above-mentioned pattern of fuel burnup errors in the CANDU reactor core is then revealed, e.g., if the core simulation enters into a transient mode. One representative case of such transient simulations, when the fuel burnup errors affect substantially the desired flux solutions, could be counted for the load-following simulations, which undergo through appreciable flux distortions in the core due to the strong neutron-absorbing xenon effect and also the adjuster rod movements for a period of several days.

Improving and/or predicting the fuel bundle irradiations as accurate as possible will result in several practical benefits in the context of economic and safe operation of reactors. In this context, it would not be unfair to claim that as one approach to improve the accuracy of fuel burnup predictions, the real-time concept based direct simulation of RRS actions and the subsequent use of 14 zone controller levels as well as the eventual update of reactivity device positions as input for the time-dependent core simulations should be performed, so that more realistic following of routine reactor operations could be explicitly represented in time and consequently the accuracy of fuel burnup predictions could be accordingly improved.

The fuel irradiations stored in the data-base of reactor physics codes are the first-step quoted clue and directly mirrored evidence for the daily selection of channels to be refuelled, and this refuelling process will steer to some extent the long-run outcome of neutronic characteristics with respect to the spatial distribution of neutron importance in the core that is related to the overall stability of core behaviour including the controllability of local power distributions. Simply speaking, the more accurate fuel burnup predictions should be considered as the most acceptable argument for the fuel management process.

One other area where the direct RRS actions coupled with the time-dependent core simulations should be accepted as compelling necessity is the ROP trip assessments. The over nine hundred case-dependent (core configurations) flux shapes based static ROP trip assessment methodologies are currently in place for the determination of Hand Switch Positions during the reactor operations. These steady-state generated flux shapes are based upon the core configurations with the subjectively cast (for most cases uniform) zone levels. By performing the time-dependent core simulations with RRS on starting from a given steady-state condition to the time-point when the final core configurations would be equivalent to the corresponding steady-state core configurations that are currently categorized over nine hundred flux shapes, as mentioned above, would enhance the reliability of the decision making process for the ROP Hand Switch selections. By assessing the ROP trip during the time-dependent core simulations with RRS on more realistic, reliable and credible margin to trip setpoints might be gained and could be turned out to increase the trip margins by eliminating the currently imbedded uncertainties in the steady-state simulations and prediction methodologies.

Carrying out the time-dependent core physics simulations with RRS on could be a very lengthy process, even though the benefits and importance could be argued, for the practical cases of routine following of the reactor operations due to the small time-step size of $\Delta t=0.5$ s that is set for the bulk control of reactor power. Thus, an attempt has been made in the present study to identify the feasibility of shortening the actual computing time without significant loss of accuracy in the simulation results by using a larger time-step size of $\Delta t=1.0$ s, and also to identify the possibility of practical applications of such simulations for the safety analysis of various accidents of CANDU 6 reactors, such as, LBLOCA, SBLOCA, In-CORE LOCA, LOR and moderator accidents, which could be covered in a relatively short time span, compared to the following of daily routine reactor operations, of over several hundred seconds in terms of RRS actions.

The simulation cases presented here are the moderator drain accidents followed by LBCOCA. The moderator drain accidents undergo top-to-bottom flux tilts which cause the strain RRS performance. Thus, it is deemed that such accident scenarios could be used as the justifiable test cases to verify the practical applicability of time-dependent core simulations with RRS on, even by using a larger time step-size of $\Delta t=1.0$ s.

2. Fuel Burnup Distribution – RFSP-IST Model

The fuel burnup distribution of RFSP-IST CANDU 6 model is generated by using the TAVEQUIV module [1]. The burnup zones in the core are subdivided into eight regions according to the design model. The standard eight bundle bi-directional refuelling scheme is applied with the average zone

level of AVZL=50% distributed uniformly in 14 zones. The SCM fuel tables are generated by using WIMS Utilities [7]. The WIMS-IST lattice parameters used for the fuel table generations are as follows; Reactor Power = 100% FP or 33.4902 W/g of Initial HE, Moderator Temp = 69 °C, Fuel Density = 10.4919 g/cm³, Avg. Fuel Wt. = 19.135 (kg U)/BND, Coolant Purity = 99.000 at%, Moderator Purity = 99.833 at% and Moderator Poison = 0 ppm. The pressure tube creep is not accounted for in generating fuel tables.

3. Mesh Spacing Layout (48x40x40) – RFSP-IST Model

The number of mesh intervals in x-, y- and z-directions is set to 48x40x40, respectively (see Table 1). This model is the same one as Model S used in [8] and can be used both for steady-state and SDS1/2 associated transient simulations without changing the mesh layouts. The first three mesh intervals in x-, y-directions, which are equivalent to x, y = 0-68.525 cm, cover the reflector region, respectively. In y-direction, the mesh intervals between y=68.525-97.100 and y=97.100-125.676 cover the lattice cells containing the fuel channel Row A and B, respectively. The z-direction mesh spacings are derived from the basic mesh spacing of 49.53 cm corresponding to the fuel bundle length, such that all the reactivity device boundary surfaces in z-direction become coincident with one of the 40 mesh lines.

Table 1 Mesh Spacing Layout (48x40x40) - RFSP-IST Model
 (Mesh Sizes Are in Centimetres)

X-Direction		Y-Direction		Z-Direction	
(1)	0.0000	(1)	0.0000	(1)	0.0000
(2)-(47)	11.3750	(2)-(39)	11.3750	(2)-(39)	49.5300
(3)-(46)	28.5750	(3)-(38)	28.5750	(3)-(38)	47.6500
(7)-(42)	14.2875	(4)-(37)	14.2875	(4)-(37)	1.8800
(48)	0.0000	(6)-(9)	28.5750	(5)-(36)	16.9100
		(16)-(16)	28.5750	(6)-(35)	26.2100
		(19)-(22)	28.5750	(7)-(34)	5.0000
		(25)-(25)	28.5750	(8)-(33)	1.4100
		(32)-(35)	28.5750	(9)-(32)	17.3800
		(40)	0.0000	(10)-(31)	6.2100
				(11)-(30)	20.2350
				(12)-(29)	5.7050
				(13)-(28)	24.0600
				(14)-(27)	10.0000
				(15)-(26)	9.76500
				(16)-(25)	5.70500
				(17)-(24)	4.2100
				(18)-(23)	20.5550
				(19)-(22)	9.7650
				(20)-(21)	15.0000
				(40)	0.0000

4. PHTS and SHTS Thermalhydraulics - CATHENA Model

The thermalhydraulic behaviour of the primary and secondary heat transport system (PHTS and SHTS) is simulated using the CATHENA full circuit model that is designed for the safety analysis of the Wolsong-1 refurbished reactor. The multiple (a total of twenty-eight groups or seven groups in each core pass 1-4) average channel model [9] is incorporated into the CATHENA input so that the

coolant density and temperature and the fuel temperature can be transferred from the CATHENA output to the CERBERUS input to be used as local parameters for the flux iterations [1]. The CERBERUS calculated bundle and channel powers are then summed up into twenty-eight average channel groups and fed back into the CATHENA input for the next time-step simulation.

For the moderator drain accident simulations presented here, the coupling between CATHENA and CERBERUS is carried out only for the steady-state cases and the steady-state local parameter distribution is then used throughout the transient simulations thereafter with RRS on. For the LBLOCA simulations the coupling between CATHENA and CERBERUS is carried out not only for the steady-state simulations, but also for the time-dependent simulations at every time-step throughout the transient with the RRS actions frozen as usual.

5. Reference Flux Distribution – Case C000R00 - ROP Trip Assessments

The RFSP-IST reference flux distribution at 100% FP is generated with the CATHENA coupling based upon the time-average equivalent fuel irradiation distribution (see Section 2). The average zone level is set to 50% fill and the CATHENA/RFSP-IST coupled iteration is carried out until the consistency between the thermalhydraulic and neutronic thermal power balance is established (say, the bundle power differences in each thermalhydraulic group converge less than 1% between the two successive iterations). During the iterations the individual zone levels are updated so that the core power distribution is obtained with minimal power tilts in x-, y- and z-direction, respectively. The flux distribution so generated will be used to calculate the detector fluxes at the 34 SDS1 ROP detector sites for the trip assessment during a transient. The trip times are calculated by using the TRIP_TIME module [1]. The simulation results for the reference steady-state case are summarized in Table 2 both for the flux and thermalhydraulic iterations. The thermal power tilt in x- (HTilt-horizontal), y- (VTilt-vertical) and z-direction (ATilt-axial) are defined as follows, respectively;

$$\text{Tilt (\%)} = (\text{High Half Core Power} - \text{Low Half Core Power}) / (\text{Total Power}) * 100.$$

Table 2 RFSP-IST/CATHENA Simulation Results for Reference Steady-State Case at 100% FP

Core Pass	RIH Temp	ROH Temp	RIH Pressure	ROH Pressure	Thermal Power(MW)			
	(Deg C)	(Deg C)	[MPa(a)]	[MPa(a)]	Core Pass	Axial	Low-Z	High-Z
1	267.48	310.83	11.09	10.07	513.31	LY-LX	258.26	257.91
2	266.32	309.15	11.05	9.84	516.92	LY-HX	258.12	257.43
3	267.67	310.93	11.09	10.08	512.64	HY-LX	258.28	256.92
4	266.20	309.09	11.05	9.83	518.74	HY-HX	257.83	256.86
HTilt(%)		VTilt(%)		ATilt(%)		Diff(%) [RFSP-CATHENA]		
RFSP	CATHENA	RFSP	CATHENA	RFSP	CATHENA	HTilt	VTilt	ATilt
-0.07	-0.06	-0.12	-0.09	-0.35	-0.16	-0.01	-0.03	-0.18
Zone Fills (%)								
Average	#1/8	#2/9	#3/10	#4/11	#5/12	#6/13	#7/14	
50.00	50.80	50.80	53.40	50.80	46.60	49.20	49.20	
	50.80	50.80	53.40	49.20	46.60	49.20	49.20	
	1-1/keff (mk)		MCP(MW)	MBP(kW)				
	0.07		6.62/O08	779.20/P06-6				

6. Initial Steady-State Condition – Case A

The initial steady-state condition to be used as the starting point for the transient simulations is derived from the reference steady-state condition that is described in Section 5. The reactor is undergone for three day’s burn process at 100% FP. During these three day’s operation six fuel channels including O17 and H08 are refuelled with fresh fuels according to the standard eight-bundle shift operations.

The flux solution is again generated with the CATHENA coupling based upon the same iteration methodology as applied to the reference case C000R00 (see Section 5). The simulation results for the initial steady-state Case A is summarized in Table 3 both for the flux and thermalhydraulic iterations. Note that MCP and MBP are located in the refuelled channel O17.

Usual practice is applied to derive the density scale based upon the best estimate value of Coolant Void Reactivity (CVR) bias for WIMS-IST [6] taken as WIMS CVR – 1.6 mk. The Margin To Trip (MTT) is obtained by subtracting CPPF=1.05 from the least value of effective trip setpoints as calculated by TRIP_TIME/RFSP-IST at the 34 SDS1 detector sites.

Table 3 RFSP-IST/CATHENA Simulation Results for Initial Steady-State Case A at 100% FP

Core Pass	RIH Temp	ROH Temp	RIH Pressure	ROH Pressure	Thermal Power(MW)			
	(Deg C)	(Deg C)	[MPa(a)]	[MPa(a)]	Core Pass	Axial	Low-Z	High-Z
1	266.77	309.72	11.03	9.92	519.41	LY-LX	257.88	257.20
2	266.95	309.51	11.02	9.90	512.30	LY-HX	257.76	258.14
3	266.87	310.13	11.06	9.97	515.91	HY-LX	257.57	257.45
4	267.00	309.58	11.05	9.90	514.20	HY-HX	257.05	258.77
HTilt(%)		VTilt(%)		ATilt(%)		Diff(%) [RFSP-CATHENA]		
RFSP	CATHENA	RFSP	CATHENA	RFSP	CATHENA	HTilt	VTilt	ATilt
0.04	0.08	0.01	-0.01	0.27	0.06	-0.04	0.01	0.21
Zone Fills (%)								
Average	#1/8	#2/9	#3/10	#4/11	#5/12	#6/13	#7/14	
50.00	52.20	52.20	49.40	50.40	50.60	47.80	47.80	
	52.20	52.20	49.40	49.60	50.60	47.80	47.80	
1-1/keff (mk)	MCP(MW)	MBP(kW)	Density Scale	MTT(%)	Detector			
-1.274	6.87/O17	801.52/O17-7	0.900503	8.830	VFD06-RE6			

7. Initial Steady-State Condition – Case B

This initial steady-state condition is basically same as Case A (see Section 6), except HTilt = -4%. The reason for the consideration of this case is that for LBLOCA analysis it is a common practice to postulate the transient from a horizontally tilted steady-state flux distribution. On the other hand, this case would also be deemed to be well qualified for the performance test of the interfacial code being used to emulate the RRS actions in the context of coping with the appreciable flux tilts during the progression of transients.

The flux solution is again generated with the CATHENA coupling. The average zone level is set to 50% fill and the CATHENA/RFSP-IST coupled iteration is carried out by updating the 14 zone fills

individually so that the core power distribution is obtained with HTilt = -4% and the minimal VTilt= \sim 0% and ATilt= \sim 0%, respectively. The results of initial steady-state simulations for Case B are summarized in Table 4 both for the flux and thermalhydraulic iterations. Note that MCP and MBP are located in the refuelled channel H08.

Table 4 RFSP-IST/CATHENA Simulation Results for Initial Steady-State Case B at 100% FP with HTilt = -4%

Core Pass	RIH Temp	ROH Temp	RIH Pressure	ROH Pressure	Core Pass	Thermal Power(MW)		
	(Deg C)	(Deg C)	[MPa(a)]	[MPa(a)]		Axial	Low-Z	High-Z
1	266.86	310.37	11.12	10.01	494.23	LY-LX	269.25	268.39
2	266.59	310.46	11.12	10.02	494.12	LY-HX	246.47	246.57
3	267.08	310.39	11.12	10.01	535.60	HY-LX	267.89	267.56
4	266.89	310.25	11.12	9.99	537.49	HY-HX	247.04	248.26
HTilt(%)		VTilt(%)		ATilt(%)		Diff(%) [RFSP-CATHENA]		
RFSP	CATHENA	RFSP	CATHENA	RFSP	CATHENA	HTilt	VTilt	ATilt
-3.98	-4.11	0.01	0	0.05	0.01	0.13	0.01	0.05
Zone Fills (%)								
Average	#1/8	#2/9	#3/10	#4/11	#5/12	#6/13	#7/14	
50.00	37.93	37.93	49.40	50.40	50.60	62.07	62.07	
	37.93	37.93	49.40	49.60	50.60	62.07	62.07	
	1-1/keff (mk)	MCP(MW)	MBP(kW)	Density Scale	MTT(%)	Detector		
	-1.249	7.11/H08	806.61/P06-6	0.900476	2.947	VFD05-RE2		

The density scale and MTT are calculated in the same way as described in Section 6 for Case A. Even with HTilt = -4%, the consistency between the RFSP-IST and CATHENA predicted thermal power balance shows the practically excellent agreement.

8. RRS Parameters

The RRS algorithm parameter values used in the present study are listed below. The values are practically the same as the design values of RRS for CANDU 6 reactors. Since the RRS simulations carried out here are for more or less parametric investigations, the sensitivity of the results depending on the use of various set of RRS parameters is not given here. In other words, no reactor unit-specific RRS parameters are preferred so that the results presented here could be interpreted in generic view.

Zone	Control Level Gain Factor A	KH = 0.6
Zone	Control Level Gain Factor B	KL = 0.1
Flux Tilt	Control Level Gain Factor	KT = 3.0
Bulk Power Control	Gain Factor	KP = 16
Zone Valve Lift Bias		BIAS(I) = 0.6, for I = 1, 14.

For safety analysis, the setback and stepback modes are not usually credited. Thus, these modes are not applied here.

9. DO_NOTHING Qualifications

The quality of simulation results obtained by using CERBERUS with RRS on will depend on the stable and reliable performance of a computer program that interfaces with CERBERUS. As transient proceeds, the updated 14 zone fills as well as reactivity device positions predicted by the interfacial program are fed into the CERBERUS input for the flux calculations at the next time-step. Thus, before any actual accident related transient simulation is conducted, the combined set of simulation tools should be thoroughly tested in the first place, and it can be done normally based upon the DO_NOTHING approach.

As the terminology implies, the DO_NOTHING simulations are performed without any core system reactivity perturbations and must not show any noticeable change in flux shapes, zone levels and tilts as well as in dynamic core system reactivity for an extended period of transients that could be equivalent to the time period during which the reactivity perturbation due to the relevant accident transient scenarios would be the dominant source of reactivity changes contributed into the core system. Thus, there must not be any reactivity device movements, such as, adjuster rods and mechanical control absorbers, due to the RRS actions during the DO_NOTHING transient simulations, except the very slowly changing zone levels within acceptable ranges. The zone level distributions must not transit into the distorted tilt patterns so that the local flux shapes do persist to remain practically the same as in the case of the initial flux distributions existing before the start of DO_NOTHING simulations.

It is assumed that the changes in xenon and delayed neutron precursor concentrations during a transient are negligible and the initial steady-state equilibrium concentrations are held unchanged throughout the transients. The DO_NOTHING transient simulations are carried out for the period of $t=0-495$ s and the results are summarized in Tables 5-1,2,3,4,5 for the initial steady-state condition of Case A and B (see Sections 6 and 7), respectively.

Table 5-1 Core System Reactivity RHO Change (mk)

	Time-Step Size $\Delta t=0.5$ s				Time-Step Size $\Delta t=1.0$ s			
	Max. Negative	Time (s)	Max. Positive	Time (s)	Max. Negative	Time (s)	Max. Positive	Time (s)
Case A	-0.002039	445.50	0.003602	18.00	-0.003766	401.00	0.005447	12.00
Case B	-0.001879	369.50	0.003420	21.00	-0.001719	3.00	0.002410	21.00

Table 5-2 Reactor Total Power Change (%)

	Time-Step Size $\Delta t=0.5$ s				Time-Step Size $\Delta t=1.0$ s			
	Max. Negative	Time (s)	Max. Positive	Time (s)	Max. Negative	Time (s)	Max. Positive	Time (s)
Case A	-0.031000	6.50	0.028600	1.00	-0.027600	5.00	0.086800	76.00
Case B	-0.045600	5.50	0.028100	1.00	-0.086800	11.00	-0.012100	114.00

In Table 5-1, the core system reactivity changes given relative to $t=0$ s are obtained by using $\Delta t=0.5$ and 1.0 s, respectively. Both the maximum changes in negative and positive values are given and the corresponding times when these values occurred. As can be seen, the core system reactivity changes

are practically negligible and the results obtained by using $\Delta t=1.0$ s are very closely comparable to the results obtained by using $\Delta t=0.5$ s.

The changes in reactor total power (100% RTP = 2061.4 MW(th) at $t=0$ s) are given in Table 5-2. In this case, the changes behave very similarly as in the case of core system reactivity changes except for Case B with $\Delta t=1.0$ s, where the RTP maximum positive change shows a negative value. Note that the total RTP stays at the initial 100% FP throughout the transients as a result of the RRS actions. This observation vindicates the soundness of the interfacial program being used here between the CERBERUS simulations and the RRS actions. It is worth mentioning that the initial flux shape with the side-to-side power tilt (HTilt = -4%) exerts very little effects on the progress of flux shapes during the DO_NOTHING transient simulations.

The changes in the 14 zone powers relative to the each individually corresponding initial zone powers at $t=0$ s are given in Table 5-3. The values shown are taken out of all 14 zone power values. The pattern of changes are consistent for the case of using $\Delta t=0.5$ and 1.0 s and for Case A and B, respectively. Note that in this case the changes for Case B with $\Delta t=1.0$ s reveal considerably larger values compared to the case of using $\Delta t=0.5$ s although the absolute values are small in magnitude to convey any significant meaning for the practical interpretations. It can be observed again that the interfacial program between CERBERUS and RRS is soundly functioning.

In Table 5-4, the changes in average zone fill (%) (initially 50% fill at $t=0$ s) are shown. The values are the differences between the initial average zone fill and the average zone fill during the transients. Note that the results produced by using $\Delta t=1.0$ s show slightly larger values compared to the case of using $\Delta t=0.5$ s, and the similar observations can be made between Case A and B. The overall observation vindicates again the soundness of the interfacial program being used between CERBERUS and RRS.

The final results for the DO_NOTHING tests are shown in Table 5-5 for the changes in each individual zone fill (%). Similar to the case of zone power changes, the values given are taken out of all 14 zone fill values.

Table 5-3 Zone Power Change (%)

	Time-Step Size $\Delta t=0.5$ s				Time-Step Size $\Delta t=1.0$ s			
	Max. Negative	Time (s)	Max. Positive	Time (s)	Max. Negative	Time (s)	Max. Positive	Time (s)
Case A	-0.081700	445.50	0.079000	322.00	-0.113600	77.00	0.197500	76.00
Case B	-0.353000	75.50	0.377700	77.00	-0.575700	96.00	0.515600	97.00

Table 5-4 Average Zone Fill Change (%)

	Time-Step Size $\Delta t=0.5$ s				Time-Step Size $\Delta t=1.0$ s			
	Max. Negative	Time (s)	Max. Positive	Time (s)	Max. Negative	Time (s)	Max. Positive	Time (s)
Case A	-0.130001	455.50	0.010002	1.00	-0.139999	403.00	0.000000	
Case B	-0.229999	392.50	0.010002	1.00	-0.250000	388.00	0.029999	2.00

Table 5-5 Zone Fill Change (%)

	Time-Step Size $\Delta t=0.5$ s				Time-Step Size $\Delta t=1.0$ s			
	Max. Negative	Time (s)	Max. Positive	Time (s)	Max. Negative	Time (s)	Max. Positive	Time (s)
Case A	-0.350004	475.50	0.140002	64.00	-0.689998	427.00	0.290000	68.00
Case B	-1.310003	336.50	0.880000	71.00	-1.819998	463.00	1.310000	51.00

The changes for Case B show several times larger values compared to the case of Case A. This implies that the initially distorted flux shape (HTilt = -4%) at t=0 s contributes more to the accumulation of numerical uncertainties in the RRS actions with the progression of transients. The largest absolute value is ~1.82%, and considering the numerical complexities associated with the transient simulations of core physics with RRS on, the departure of this magnitude from the initial zone fill distributions could be harmlessly absorbed. Note that the changes in 14 zone fills show a similar pattern as in the case of 14 zone powers (see Table 5-3) so that the changes for Case B with $\Delta t=1.0$ s reveal considerably larger values compared to the case of using $\Delta t=0.5$ s, although the absolute values are again small in magnitude to convey any significant meaning for practical interpretations.

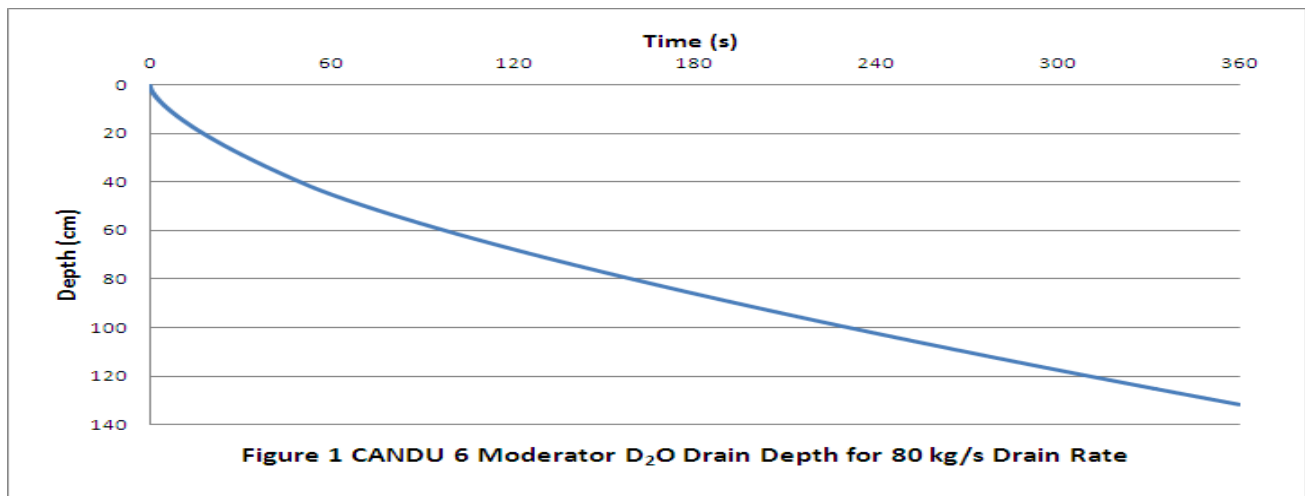
Based upon the DO_NOTHING simulations as given and discussed throughout Tables 5-1,2,3,4,5, the interfacial program being used in the present study can be qualified for the core physics transient simulations, even with the strain demand in the RRS performance and using a larger time-step size of $\Delta t=1.0$ s.

10. Transient Simulation Cases

For the purpose of sensitivity studies depending on the initial steady-state conditions and the time-step sizes used for RRS, the cases studied are classified here. The transient type is the moderator drain accident followed by LBLOCA, i.e., a severe dual accident, which is deemed to be characterized by appreciable flux tilts during the progression of transients. The first part of such accident type with slowly but gradually growing top-to-bottom flux tilts then in turn puts the RRS actions in strain demand and furthermore, especially, the LBLOCA transients are more severely tested due to the existence of top-to-bottom as well as side-to-side flux tilts before the start of LOCA compared to the cases when only side-to-side flux tilts initially exist.

For the moderator drain accidents, the drain rate considered here is 80 kg/s, which is accepted as a standard drain rate to be applied to CANDU 6 safety analysis, whereas for the LBLOCA ROH 100% break cases are quoted.

The drain depth vertically measured in centimetres from the top of reactor calandria or RFSP-IST mesh model to the moderator D₂O level surface is simply calculated based upon the geometric layout of CANDU 6 reactor calandrias including the notch portion. For simplicity, all the structures including the fuel channels that are not occupied by D₂O volumes are not accounted for the estimate of drain depth in time with the progression of moderator inventory loss accident. No thermalhydraulic code, which would normally, e.g., accounts for the redistribution of pressure in the moderator calandria tank as well as the moderator heat load during transients, is used to estimate the drain depth. The drain depth used for the simulations is graphically shown in Figure 1 for the time interval of t=0-360 s.



Each transient case is identified by a label consisting of seven characters CqqqArs or CqqqBrs, in which the uppercase A and B correspond to the initial steady-state conditions, Case A and B, respectively (see Sections 6 and 7). The three letters qq q represent the moderator drain rates, either 000 (no moderator drain) or 080 for 80 kg/s drain rate, respectively. The letter r indicates the depth vertically measured from the top of RFSP-IST mesh model to the moderator level surface, above which the moderator liquid is replaced by gas and/or air due to drain, with the progression of moderator drain accidents as follows (refer to Table 1), and the last letter s is set to 0 (no RRS actions), 1 ($\Delta t=0.5$ s with RRS on) or 2 ($\Delta t=1.0$ s with RRS on);

- r = 0 : No moderator drain accident, i.e., no RRS on. LBLOCA starts without moderator drain,
- r = 1 : Moderator drain depth reaches 39.950 cm or the bottom of 3rd mesh interval of RFSP-IST model (see Table 1),
- r = 2 : Moderator drain depth reaches 68.525 cm or the bottom of 4th mesh interval of RFSP-IST model (see Table 1). This depth is coincident with the interface between the reflector and channel Row A lattice of RFSP-IST model,
- r = 3 : Moderator drain depth reaches 97.100 cm or the bottom of 5th mesh interval of RFSP-IST model (see Table 1). This depth is coincident with the interface between the channel Row A and B lattices of the model. Note that the fuel channel Row A is completely uncovered due to the moderator liquid drain, and
- r = 4 : Moderator drain depth reaches 125.675 cm or the bottom of 6th mesh interval of RFSP-IST model (see Table 1). This depth is coincident with the interface between the channel Row B and C lattices of the model. Note that in this case the fuel channel Row A and B are completely uncovered due to the moderator liquid drain.

There are all together 18 transient cases. Note that there are only two cases without moderator drain, namely, C000A00 and C000B00. For the cases with C080Ars and C080Brs, the moderator drain accidents proceed with RRS on until the drain depth becomes one of the cases r = 1,2,3,4. During the transient period with RRS on, the time-step size used for the simulation of moderator drain accidents corresponds to one of the two cases, s = 1 or 2, i.e., either $\Delta t=0.5$ or 1.0 s, respectively.

It is worth mentioning that due to the fixed size of time-steps, $\Delta t=0.5$ or 1.0 s, the actual drain depth at the end of any time-step may not be exactly coincident with the above-given mesh lines of the RFSP-IST model. Thus, the time points during transients at which the drain depths become nearest to the one of the above-given mesh line are quoted in the present work.

11. Results of Moderator Drain Accident Transient Simulations

Since the primary interest of the present study is to investigate the LBLOCA behaviour with respect to the initial steady-state conditions used for the start of LBLOCA, which are initiated from the previously existing flux shapes as progressed by the moderator drain accidents with RRS on by using $\Delta t=0.5$ and 1.0 s, the trip assessment is not carried out during the progression of moderator drain transients by simply assuming that none of the four shutdown systems, namely, ROP/Rate-Log SDS1/2, would have been triggered.

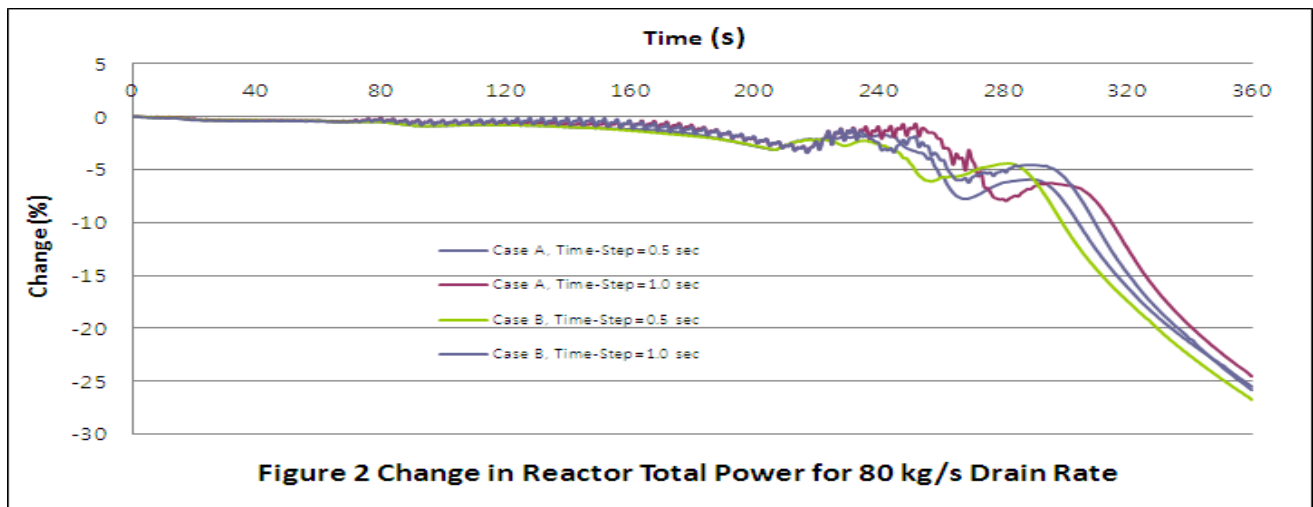


Table 6-1 Starting Time (s) of Adjuster Rod Withdrawal for 80 kg/s Drain Rate

	Case A		Case B	
	Bank A	Bank B	Bank A	Bank B
$\Delta t=0.5$ s	206.50	257.50	206.50	251.50
$\Delta t=1.0$ s	217.00	267.00	217.00	263.00

The changes in RTP with 80 kg/s drain rate are graphically shown in Figure 2 for the transient period of $t=0-360$ s. For this case the drain depth at $t=360$ s has already passed through the bottom of the channel Row B lattice. The starting times of adjuster rod withdrawals are also given in Table 6-1.

Note that the starting time of the adjuster Bank A withdrawal are the same for Case A and B, though the time is deferred by 10.50 seconds for $\Delta t=1.0$ s compared to the cases of $\Delta t=0.5$ s. This observation indicates that the results obtained by using $\Delta t=1.0$ s are as accurate as in the case of using $\Delta t=0.5$ s with respect to Case A and B comparisons. The time intervals between the adjuster Bank A and B withdrawals are 51.00, 50.00 and 45.00, 46.00 seconds for using $\Delta t=0.5$ and 1.0 s, respectively. Thus, it seems that the differences between the adjuster Bank A and B withdrawal

starting times (51-50 and 45-46, i.e., 1 second) are not appreciably affected by the initially distorted flux shape (Case B with HTilt = -4%). Again, the results between the cases using $\Delta t=0.5$ and 1.0 s appear to be within the practically acceptable range, and it could be furthermore observed that using $\Delta t=1.0$ s the reactor power decreases slower compared to the case of using $\Delta t=0.5$ s so that it would be more conservative because it would take longer until the reactor operation enters eventually into the self-shutdown mode due to the moderator drain.

The maximum differences in the RTP changes between the case of using $\Delta t=0.5$ and 1.0 s are 0.87 and 0.96% for Case A and B, respectively, until the time point before the adjuster Bank A is withdrawn, and after that the differences increase appreciably to 4.62 and 4.88% at $t=310$ and 304 s, respectively, with a slightly larger value for Case B. Thus, as far as the prediction of RTP is concerned it could be confirmed that the results obtained by using a larger time-step size of $\Delta t=1.0$ s for the RRS actions instead of $\Delta t=0.5$ s would be practically acceptable, if there are no adjuster rod movements during transients.

From Figure 2 it is obvious that the RTP is being held very closely to its initial value of 100% FP for a prolonged period of transient time. However, this tendency could not be sustained further as the moderator drain continues and the RRS system is no longer capable of making up the core system reactivity deficit due to the continuing moderator inventory loss, and the reactor operation finally enters into the self-shutdown mode.

For further information, the adjuster rod withdrawals in centimetres are given in Table 6-2 at the times when the moderator drain depth reaches the mesh lines $r = 1,2,3,4$, respectively (see Section 10). According to the RFSP-IST mesh model the withdrawal distance of -554.30 cm corresponds to the out-of-core adjuster rod positions.

Table 6-2 Adjuster Rod Withdrawals in Centimetres for 80 kg/s Drain Rate

Time-Step	Mesh Line	Time (s)	Case A		Case B	
			Bank A	Bank B	Bank A	Bank B
$\Delta t=0.5$ s	r = 1	62	0	0	0	0
$\Delta t=1.0$ s	r = 1	62	0	0	0	0
$\Delta t=0.5$ s	r = 2	138	0	0	0	0
$\Delta t=1.0$ s	r = 2	138	0	0	0	0
$\Delta t=0.5$ s	r = 3	238	-189.75	0	-217.41	0
$\Delta t=1.0$ s	r = 3	238	-134.03	0	-136.25	0
$\Delta t=0.5$ s	r = 4	354	-554.30	-554.30	-554.30	-554.30
$\Delta t=1.0$ s	r = 4	354	-554.30	-554.30	-554.30	-554.30

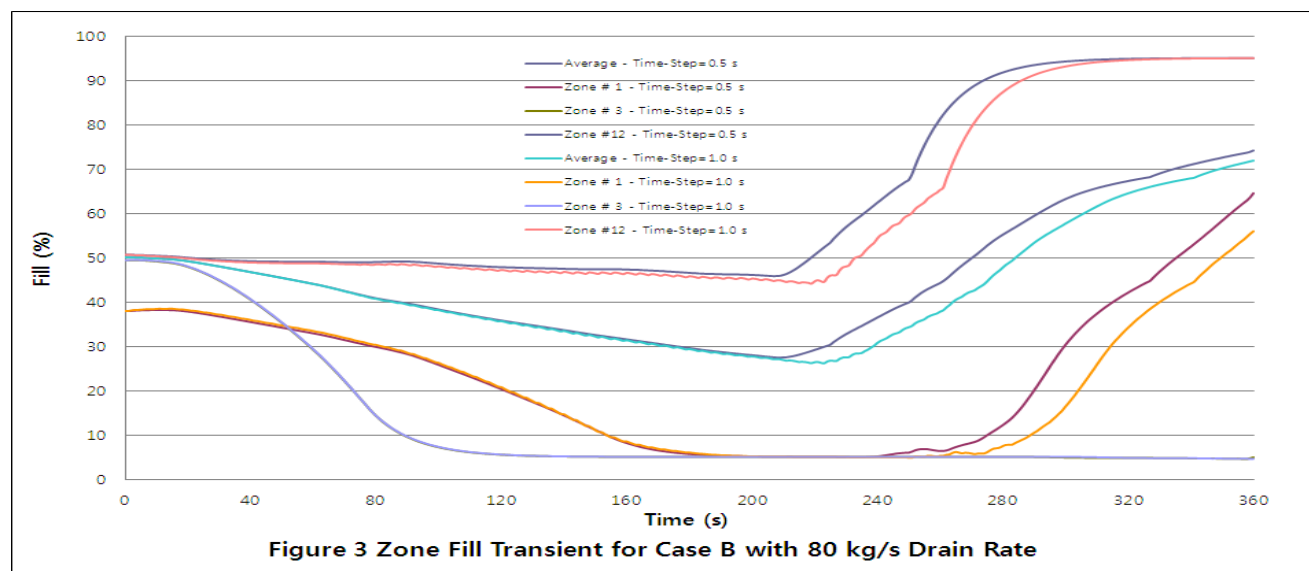
For the accuracy of zone fill predictions, the simulation results reveal that the average and 14 zone fills as obtained by using the time-step size of $\Delta t=0.5$ and 1.0 s for Case A and B are in agreement within 1% differences, respectively, until the adjuster rods are withdrawn. The average zone fills are decreasing to compensate the core system reactivity loss due to drain until the adjuster rods are withdrawn, and then thereafter the fills tend to flood to counteract against the excessive core system positive reactivity inserted by withdrawing the adjuster rods. The fills in the upper zones (#1/8, #3/10 and #6/13) drop rapidly and tend to drain whereas it is opposite for the lower zones (#2/9, #5/12 and

#7/14) which tend to flood due to the growing top-to-bottom power tilts. The largest differences in zone fills are found to be -11.02% in zone #1 between C080A42 and C080A41 and -15.92% in zone #14 between C080B32 and C080B31 for Case A and B, respectively. The large offset between the cases of using $\Delta t=0.5$ and 1.0 s are attributed to the different starting time of adjuster bank withdrawals.

The average and individual zone fill transients (zone #1, 3, 12) are graphically shown in Figure 3 for Case B. The cases of using the time-step size of $\Delta t=0.5$ and 1.0 s are displayed together for comparison purposes. As expected, the curves for the different time-step sizes are closely in accordance until the adjuster rod withdrawals, and the gap between the two sets of curves begin to narrow due to the newly settled flux shapes with the complete removal of the adjuster Bank A and B.

Note that the top zone #3 fill reaches to its design limit value of 5% long before the adjuster rod withdrawal due to the rapid decrease of power in that zone, and unchanged throughout the transient. The average zone fill drops gradually in time until the adjuster rod removal, and starts to increase in order to compensate the excess positive core system reactivity inserted by the adjuster rod removals.

A similar observation could be made for the bottom zone #12. However, its zone fill increase rate is larger compared to the average fill rate, and this phenomenon is attributed to the fact that with the growing top-to-bottom flux tilts the bottom zones are filled faster to suppress the accordingly growing overpower in the bottom zones. Similar to zone #3, the fill in zone #12 is flooded to its design value of 95% fill at a certain time point and remains unchanged from thereon throughout the transient. The other top zone #1, which is the top one of the side pair of two zones #1, 2, drains also gradually with the progression of transient but with lesser drain rate compared to zone #3.



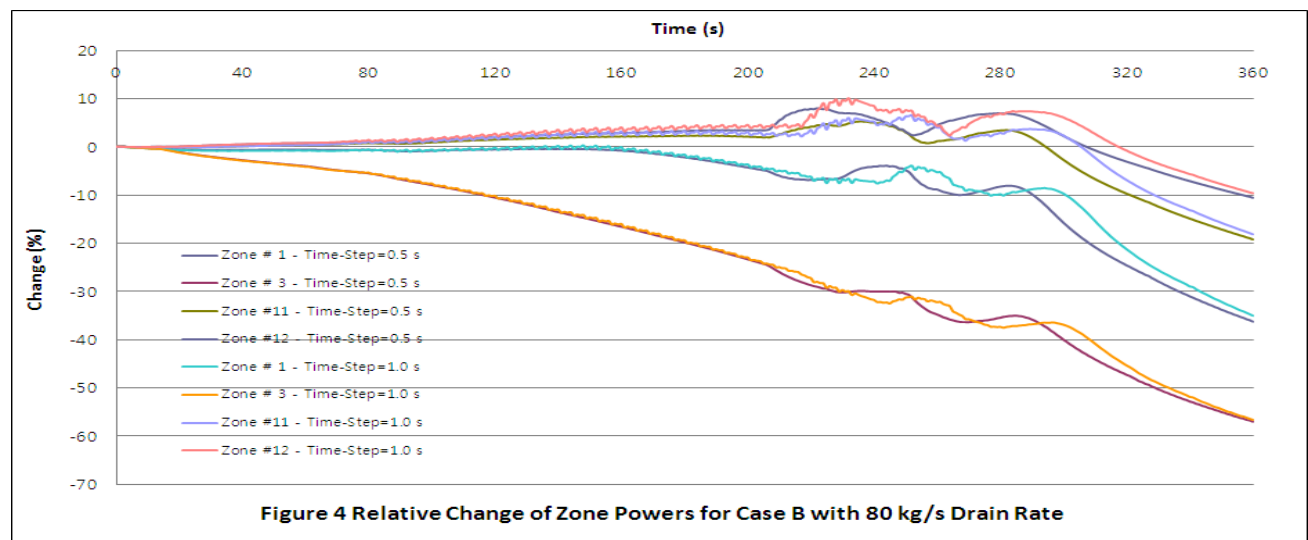
Note that the fill in zone #1 is also eventually drained down to its limit value of 5%, but then starts to be restored back beyond its initial fill because the other top and bottom zones #3/5 are drained and flooded, respectively, but have no room for further drain and fill, whereas the zone #1 has been left with room to accommodate the RRS demand of differential filling of water. The above-observed

behaviour of zone fills is also valid for the zones of opposite locations, i.e., zone #1/8, #3/10 and #5/12.

From the comparisons between the results obtained for Case A and B, it turned out that the initial condition of Case B with the side-to-side flux tilt does not exert any appreciable impact on the transient of zone fills.

The change of zone powers (zone #1/3/11/12) relative to the initial zone powers at $t=0$ s are graphically shown in Figure 4 for Case B and the cases of using the time-step size of $\Delta t=0.5$ and 1.0 s are displayed together for the comparison purposes.

Similar to the zone fill transients, the 14 zone power changes (%) relative to the initial zone powers at $t=0$ s are also compared between the results obtained by using the time-step size of $\Delta t=0.5$ and 1.0 s for Case A and B, respectively. The differences are again in agreement within 1% differences, as in the cases of zone fill transients, until adjuster rods are withdrawn. The powers in the upper zones (#1/8, #3/10 and #6/13) drop monotonically and the zone #3/10 powers decrease most rapidly. The powers in the lower zones (#2/9, #5/12 and #7/14) including the middle zones (#4/11) increase to compensate the power decrease in the upper zones, but then decrease with the drop of RTP that is caused by the uncovering of fuel channels with the further dropping of moderator levels. The largest differences are found to be 2.20% in zone #12 between C080A32 and C080A31 and 3.02% in zone #14 between C080B32 and C080B31 for Case A and B, respectively, and these differences are considerably smaller compared to the cases of zone fills, and the reason for this is attributed to the fact that the zone powers are the spatially integrated quantities yielded with some cancellations of errors.



As expected, the curves for the different time-step sizes are closely in accordance until the adjuster rod withdrawals, and the gap between the two sets of curves begin to narrow due to the newly settled flux shapes with the complete removal of adjuster Bank A and B, and the two curves for the different time-step sizes eventually merge together with the further progression of transients.

Note that the top zone #3 power decreases sharply due to the rapid flux depression in the upper region of core caused by the loss of D₂O moderator. Furthermore, the power in zone #1 hardly exceeds its initial value whereas the powers in zones #11/12 increase due to the growing top-to-bottom flux tilts. The largest relative change in zone powers occurs in zone #7 with 11.07% and 11.43% at t=282 and 291 s for $\Delta t=0.5$ and 1.0 s, respectively. Using $\Delta t=1.0$ s the zone power predictions become slightly more conservative compared to the case of using $\Delta t=0.5$ s. The zone #1, which is the top one of the side pair of two zones #1/2, experiences the least change in zone power compared to the other zones. The above-observed behaviour of zone powers is also valid for the zones of opposite locations, i.e., zone #1/8, #3/10, #4/11 and #5/12.

From the comparisons between the results obtained for Case A and B, it turned out that the initial condition of Case B with the side-to-side flux tilt does not exert any appreciable impact on the transient of zone powers, and the transient behaviors of Case A and B actually exhibit very similar patterns as in the cases of zone fill transients.

12. LBLOCA Initial Steady-State Conditions

The initial steady-state conditions to be used as the starting points for the transient simulations of LBLOCA are derived from the transient states of moderator inventory loss accidents with 80 kg/s drain rate that are presented in Section 11, and set up for Case A and B with the reactor configurations consisting of 14 zone fills as well as adjuster Bank A and B positions as predicted by the CERBERUS simulations with RRS on, respectively. The CATHENA/RFSP-IST coupled steady-state solutions are iteratively obtained until the thermalhydraulic and neutronic thermal power balances are achieved within the desired accuracy, say, the convergence of group bundle powers within 1% differences between the two successive iterations.

The steady-state simulation results reveal that the balance between the RFSP-IST (Neutronic) and CATHENA (Thermalhydraulic) thermal power calculations are in excellent agreement and in most cases the relative differences are less than 1%. The maximum difference is turned out to be -1.18% for C080B42 and the reason for this could be attributed to the channel average grouping methodology that appears to be unable to accurately cope with the appreciable top-to-bottom power tilts.

In Table 7, the change in excess core system reactivity $\Delta\rho(\text{mk})$ is calculated relative to C000A00 and C000B00, respectively. As can be seen, the RRS actions are capable of controlling $\Delta\rho$ closely equal to zero until the adjuster rods are removed (drain depth $r = 3$, see Section 10). Furthermore, it is clearly seen that the excess core system reactivity drops sharply when the channel Row B is completely uncovered even with the adjuster Bank A and B fully pulled out, so that the reactor operation finally enters into the self-shutdown mode. The margin to trip (MTT) decreases as the top-to-bottom flux tilt (VTilt) grows. However, it increases again with the drop in RTP due to the continuing moderator inventory loss. It is likely that SDS1 ROP trip would occur when the drain depth starts to pass through the boundary between the reflector and fuel channel Row A lattice. Note that the difference in MTT between C080A31 and C080A32 as well as C080B31 and C080B32 show large values, which are to be attributed to the different starting time of adjuster rod removals.

For Case A, the location of detector (VFD06-RE6, in Table 3) which has the minimal value of effective trip setpoints is initially in the bottom region of core. After the moderator drain started, this location is shifted to the top region of core and it moves downwards as VTilt grows. For Case B, the location of detector (VFD05-RE2, in Table 4) which has the minimal value of effective trip setpoints is initially in the upper region of core due to the existing side-to-side flux tilts. Note that this location stays still in the upper region of core during the most period of transients, even after the moderator drain started and VTilt grows.

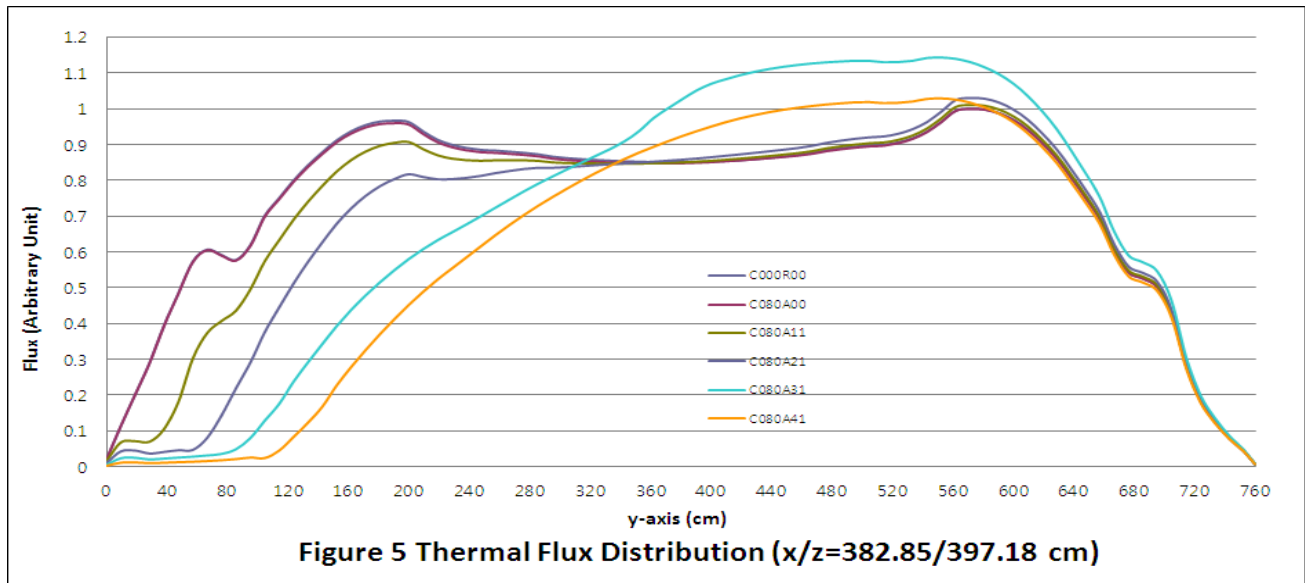
Table 7 LBLOCA Initial Steady-State Conditions with 80 kg/s Drain Rate based upon RFSP-IST/CATHENA Simulations

Case ID	RP	$\Delta\rho$	MTT	MCP	MBP	Density	HTilt(%)		VTilt(%)		ATilt(%)		Diff(%) [N-Th]			
	(FP%)	(mk)	(%)				Detector	(MW)	(kW)	Scale	N	Th	N	Th	N	Th
C080A11	99.58	-0.02	5.632	VFD02-RE3	6.94/O17	807.24/O17-7	0.901120	-0.01	0.04	1.41	1.38	0.03	0.10	-0.05	0.02	-0.07
C080A12	99.61	-0.01	5.775	VFD02-RE3	6.94/O17	807.81/O17-7	0.901083	-0.02	0.01	1.48	1.45	0.07	-0.01	-0.03	0.04	0.08
C080A21	99.07	0.01	-0.953	VFD02-RE3	7.09/O17	822.37/O17-7	0.900176	0.00	0.02	4.03	4.11	0.05	0.07	-0.02	-0.08	-0.02
C080A22	99.31	0.02	-0.953	VFD02-RE3	7.11/O17	824.05/O17-7	0.900167	-0.05	-0.08	4.14	4.19	0.16	0.02	0.02	-0.05	0.14
C080A31	98.23	0.18	-1.056	VFD05-RE2	7.41/O17	883.93/O17-7	0.898458	-0.31	-0.32	10.81	10.64	0.08	0.04	0.01	0.18	0.04
C080A32	98.68	0.21	3.263	VFD05-RE2	7.62/O17	893.99/O17-7	0.897851	-0.27	-0.28	12.41	12.07	0.09	0.09	0.02	0.34	0.00
C080A41	75.74	-0.50	26.984	VFD13-RE3	6.24/S10	771.65/S10-6	0.900382	-0.47	-0.50	20.50	19.60	-1.49	-1.51	0.03	0.90	0.02
C080A42	76.82	-0.50	24.956	VFD13-RE3	6.29/S10	778.77/S10-6	0.900275	-0.46	-0.49	20.10	19.27	-1.48	-1.52	0.04	0.83	0.04
C080B11	99.58	0.00	1.902	VFD05-RE2	7.07/H08	811.89/P06-6	0.901083	-3.79	-3.88	1.42	1.42	0.04	0.06	0.09	0.00	-0.03
C080B12	99.55	0.01	1.963	VFD05-RE2	7.06/H08	812.36/P06-6	0.900992	-3.77	-3.78	1.50	1.49	-0.09	0.09	0.01	0.01	-0.19
C080B21	99.08	0.05	-3.641	VFD05-RE2	7.17/O06	830.56/P06-6	0.899780	-4.10	-4.11	4.13	4.13	0.04	0.03	0.01	0.01	0.00
C080B22	99.60	0.05	-3.941	VFD05-RE2	7.20/O06	834.43/P06-6	0.899577	-4.02	-4.06	4.22	4.22	0.05	0.05	0.04	0.01	0.00
C080B31	97.60	0.18	-6.119	VFD05-RE2	7.74/M05	893.66/M05-8	0.898656	-4.39	-4.44	10.15	10.07	0.05	0.05	0.06	0.08	0.00
C080B32	97.86	0.22	0.906	VFD05-RE2	7.75/N06	893.11/O05-7	0.898806	-3.56	-3.63	12.49	12.11	0.08	0.08	0.08	0.38	0.00
C080B41	74.45	-0.52	28.988	VFD13-RE3	6.16/S10	762.44/S10-6	0.900366	-1.44	-1.21	20.83	19.92	-1.65	-1.67	-0.23	0.91	0.03
C080B42	75.53	-0.49	26.782	VFD13-RE3	6.22/S10	769.80/S10-6	0.900187	-1.62	-1.74	20.44	19.50	-1.54	-1.57	0.12	0.93	0.03

The value of maximum channel and bundle powers obtained by using $\Delta t=1.0$ s shows to be slightly more conservative compared to the cases with $\Delta t=0.5$ s. The density scale values appear to be practically uniform and consistent for all the cases. The magnitude of HTilts is little affected by the drain depths due to the RRS actions until the reactor power tends to collapse. Note that for C080B41 and C080B42 the magnitude of HTilts is overwhelmed by the excessively growing VTilts. The differences between the RFSP-IST and CATHENA thermal power tilts remain less than 1% for all the cases, which vindicate the soundness of the CATHENA/RFSP-IST coupling methodology being applied in the present study. From the observations made here, it could be conclusively stated that the using of $\Delta t=1.0$ s could also be practiced for the simulation of RRS actions in order to generate initial steady-state conditions to be used as starting points of various accident analyses of CANDU 6 reactors, such as, LBLOCA, SBLOCA, In-CORE LOCA, LOR and moderator accidents.

In Figure 5, the thermal flux distributions, normalized with the maximum value of fluxes for C000R00 along the y-axis at $x/z = 382.85/397.18$ cm, respectively, are graphically displayed for Case A. The flux peaking effects in the bottom region of core with the growing top-to-bottom flux tilts are little until the fuel channels are uncovered due to the moderator drain. When the fuel channels are uncovered, the neutron reflection effect by D₂O in the top region of core is rapidly diminishing, and the neutron loss from the core to the outside is in addition more and more

pronounced by the increasing loss of neutrons due to the neutron leakage effects. The largest flux peak occurs when the fuel channel Row A is uncovered and thereafter the flux shape starts to collapse with the further loss of moderator inventory, which then finally leads to the reactor operation into self-shutdown mode.



13. ROH 100% LBLOCA Simulation Results

The results of ROH 100% LBLOCA CATHENA/RFSP-IST coupled simulation results obtained based upon the initial steady-state conditions as given in Section 12 are summarized in Table 8, and briefly discussed here. The transient simulations are carried out by using RFSPCB Perl Script [10]. The origin of LBLOCA transient time for all the cases is reset to zero independent of the moderator drain accident time history. Thus, the shutoff rod origin time (SOT) is the SDS1 ROP trip actuation time calculated by the TRIP_TIME module of RFSP-IST, and the times given in Table 8 correspond to the time point relative to the starting time of LBLOCA, i.e., t= 0 s.

The dynamic core system reactivity as predicted by the CERBERUS simulations with RRS on for the moderator drain accidents are given as ρ_{ORRS} at the time of LBLOCA start. The LBLOCA dynamic core system reactivity determined by CERBERUS is given as ρ_{OLOCA} and this reactivity is adjusted (corrected) to ρ_{OCOR} by subtracting ρ_{ORRS} from it, so that it reflects the actual core system reactivity that would have been held up by the core system during the LBLOCA transients inherited from the previously sustaining moderator drain accidents before LBLOCA started. All the values quoted in Table 8 for ρ_{OLOCA} , RTP, MCP and MBP are the peak ones occurred during the LBLOCA transients.

Table 8 Summary of ROH 100% LBLOCA CATHENA/RFSP-IST Coupled Transient Simulation Results

Case ID	ρ_{ORRS} (mk)	SOT (s)	ρ_{OLOCA} (mk)	ρ_{OCOR} (mk)	RTP (MW)	MCP (MW)	MBP (kW)	Case ID	ρ_{ORRS} (mk)	SOT (s)	ρ_{OLOCA} (mk)	ρ_{OCOR} (mk)	RTP (MW)	MCP (MW)	MBP (kW)
---------	--------------------	---------	---------------------	--------------------	----------	----------	----------	---------	--------------------	---------	---------------------	--------------------	----------	----------	----------

C000A00	0.0000	1.1740	1.1110	1.1110	2616.2	9.38	1066.2	C000B00	0.0000	0.7330	0.6800	0.6800	2350.4	8.53	983.9
C080A11	-0.0009	1.1710	1.0600	1.0591	2556.6	9.15	1054.6	C080B11	-0.0007	0.8420	0.8870	0.8863	2424.3	9.02	1037.6
C080A12	-0.0004	1.1460	1.0540	1.0536	2550.6	9.14	1053.4	C080B12	-0.0018	0.8640	0.8940	0.8922	2426.5	9.03	1037.6
C080A21	-0.0006	0.7210	0.7130	0.7124	2336.2	8.35	973.1	C080B21	0.0011	0.5810	0.6110	0.6121	2304.7	8.62	950.8
C080A22	0.0037	0.7250	0.7400	0.7437	2362.4	8.47	987.1	C080B22	0.0146	0.5640	0.5780	0.5926	2304.1	8.58	957.2
C080A31	0.0147	1.1020	1.1580	1.1727	2598.6	10.53	1197.1	C080B31	0.0025	0.7560	0.8840	0.8865	2388.2	9.99	1152.7
C080A32	0.0392	1.1920	1.2280	1.2672	2674.9	10.95	1247.7	C080B32	-0.0127	0.7330	0.8340	0.8213	2373.9	9.91	1140.5
C080A41	-0.1893	2.0610	1.5680	1.3787	2418.4	10.84	1316.6	C080B41	-0.1974	2.1100	1.5780	1.3806	2400.0	10.82	1317.9
C080A42	-0.2023	2.0200	1.5650	1.3627	2435.1	10.88	1319.4	C080B42	-0.2115	2.0600	1.5820	1.3705	2412.0	10.84	1336.9

The maximum positive value of Rho_{RRS} is 0.0392 and 0.0146 mk for C080A32 and C080B22, respectively, which would correspond to the approximate change of average zone level of ~ 0.63 and $\sim 0.23\%$, respectively, based upon the estimate of zone controller reactivity worth of ~ 6.23 mk for CANDU 6 equilibrium core at full power. Since the maximum fill rate of CANDU 6 RRS zone controller system is known to be about ~ 1 (% fill)/(0.5 s), the above-quoted Rho_{RRS} is within a range of complete control by zone controllers at the next bulk control action, i.e., in the next 0.5 seconds. Note that the corresponding static core system excess reactivity $\Delta\rho$ given in Table 7 is 0.21 and 0.05 mk for C080A32 and C080B22, respectively, which are relatively larger compared to Rho_{RRS} .

The trip actuation time (TAT) initially becomes shorter after the moderator drain started, and thereafter becomes longer again as the moderator drain depth deepens and the fuel channels are uncovered. This phenomenon is especially more pronounced when the RTP drops below its full power level due to the uncovering of fuel channels. For the transients started with the initial side-to-side flux tilts, the TAT is in general shorter than the cases without the initial side-to-side flux tilts. The reason for this observation could be attributed to the enhanced flux ripple effects connected to more frequent rover of localized flux peaks, and, therefore, the frequencies of probabilities being enhanced, that the ROP detector fluxes would hit the trip setpoints, are also accordingly increased. Once the channel Row B is uncovered, the TAT for Case A and B are very close because in this situation the dropped RTP level contributes mainly to the determination of trip times rather than the localized flux peak (ripple) effects.

The peak Rho_{LOCA} before the channel Row B is uncovered is 1.2280 and 0.8840 mk for C080A32 and C080B31, respectively, and Case A reveals more severity compared to Case B in terms of dynamic core system reactivity. This observation suggests that the neutron leakage effects inherited from the initially existed side-to-side flux tilts appear to be overshadowed by the neutron leakage effects coming from the excessively and rapidly growing top-to-bottom flux tilts due to the on-going moderator drain.

The peak values of Rho_{LOCA} and Rho_{Cor} occur when the channel Row A and B are uncovered both for Case A and B, respectively, and these peak dynamic core system reactivity values are consistently larger compared to the reactivity values of C00A00 and C00B00, respectively. The greatest enhancements in Rho_{Cor} relative to C00A00 and C00B00 occur for C080A41 and C080B41 with 0.2677 and 0.7006 mk, which are ~ 24 and $\sim 103\%$ increases, respectively. In logarithmic ratio, C080B41 shows about $\ln[2.03/1.24] \sim 49.3\%$ enhancement more compared to C080A41. This

observation then leads to the conclusion that the dynamic core system reactivity enhancement effects during LBLOCA due to the previously sustained moderator drain accidents are much more pronounced for the initial conditions with the side-to-side flux tilts. In other words, the effects of neutron leakages during the LBLOCA transients accordingly add to the enhancements of dynamic core system reactivity.

It is important noting that Rho_{Cor} increases monotonically with the number of fuel channels being uncovered due to the moderator drain both for Case A and B, respectively. This observation then leads to a critical view that regardless of what and how it is configured in core conditions, the traveling time of shutoff rods to reach the vicinity of reacting fissile isotopes in the core must be credited as the most crucial factor to govern the outcome of LBLOCA transients.

Similar to the dynamic core system reactivity enhancements, the RTP, MCP and MBP enhancements relative to C00A00 and C00B00 are also observed, and they are 58.7 (~+2%) and 76.1 (~+3%) MW, 1.57 (~+17%) and 2.31 (~+27%) MW and 253.2 (~+24%) and 353.0 (~+36%) kW for Case A and B, respectively. It is seen here also that the enhancements are much more pronounced for the initial conditions with the side-to-side flux tilts as in the case of dynamic core system reactivity.

14. Further Works

The efforts to apply the RRS actions to follow the daily reactor operations and in parallel to use the results in order to set up the initial conditions as starting points of various relevant accident scenarios for CANDU 6 safety analysis, such as, LBLOCA, SBLOCA, In-CORE LOCA, LOR and moderator accidents, are going to be extended further with the following items that could find the immediate applications for the realistic and practical purposes;

- 1) use the time-step size of $\Delta t=2.0$ s for the RRS simulations by creating the complementary models to cope with the RRS algorithms, and in order to improve the overall computational efficiency of CATHENA/RFSP-IST coupled simulations without losing accuracy,
- 2) exploit the results of core follow Thermalhydraulic/Physics/RRS coupled simulations to correct the core fuel irradiations, and reduce the fuel burnup associated errors of physics calculations,
- 3) use the fuel burnup corrected reactor physics model to improve the ROP detector calibrations as well as the ROP trip assessments, and also use the model to develop the automated ROP detector calibration programs, and
- 4) furthermore apply the fuel burnup corrected reactor physics model to derive more reliable and accurate estimate of maximum bundle and channel power uncertainties to enhance the limiting condition of operations (LCO) and improve the fuel managements (economy) at site.

15. Conclusions

In the present study, an attempt has been made to use a larger time-step size of $\Delta t=1.0$ s, which is double the size of $\Delta t=0.5$ s that represents the normal bulk control time-step size of CANDU 6 RRS algorithm, to simulate the moderator drain accidents by using RFSP-IST/CERBERUS with RRS on. The moderator drain accident scenarios are set up to reflect the fast growing top-to-bottom flux tilts in time by postulating the accidents with 80 kg/s drain rate, and also with the initial side-to-side flux

tilts to test more severely the soundness of the interfacial program being used in the present study to emulate the RRS actions coupled with CERBERUS. The reactor configurations existing at the various moderator drain depths (levels) are quoted to establish the initial steady-state conditions to be used as the starting points of ROH 100% LBLOCA transient simulations, i.e., severe dual accident scenarios.

The results obtained from the moderator drain accident simulations by using the time-step size of $\Delta t=0.5$ and 1.0 s are analyzed, respectively, and compared against each other with respect to the relevant reactor physics and RRS aspects. From the results of comparisons, it turned out that using $\Delta t=1.0$ s could be practically accepted without any meaningful loss of accuracy. From the point of view for safety analysis, the results obtained by using $\Delta t=1.0$ s would tend to be slightly more conservative. Thus, it suggests that the RFSP-IST/CERBERUS simulations conducted here with RRS on could be further extended to carry out various accident analyses of CANDU 6 reactors, such as, LBLOCA, SBLOCA, In-CORE LOCA, LOR and moderator accidents, which would be of practical interest and importance for safety analysis related licensing submissions.

The ROH 100% LBLOCA transient simulation results reveal that the initial steady-state conditions, which are established at the various time-points during the transients of moderator drain accidents, without the initial side-to-side flux tilts lead to more conservative results compared to the cases of with the initial side-to-side flux tilts. However, the relative enhancement, as compared to the cases without the moderator drain accidents (C000A00 and C000B00), of relevant reactor physics parameters that occur during the LBLOCA transient periods, such as, the peak values of dynamic core system reactivity, RTP, MCP and MBP are much more pronounced for the initial conditions with the side-to-side flux tilts, when the moderator drain accidents are followed by LBLOCA as severe dual accidents. This fact strongly reflects the effects of neutron leakages during the severe dual accidents, which are postulated with the moderator drain accidents and LBLOCA, that add to the severity of accidents including the relative enhancement of dynamic core system reactivity during the transients.

Based upon the results obtained in the present work from the moderator drain accidents and LBLOCA severe dual accident simulations, it can be firmly concluded with a critical view that regardless of what and how it is configured in core conditions, the traveling time of shutoff rods to reach the vicinity of reacting fissile isotopes in the core must be credited as the most crucial factor to govern the outcome of LBLOCA transients.

16. Acknowledgements

The technical advice provided by Professor Emeritus Se-Kee Oh, Ajou University, Suwon, Korea, to the author, Dai-Hai Chung, during the course of the present study is hereby gratefully acknowledged.

17. References

- [1] B. Rouben, "RFSP-IST, The Industry Standard Tool Computer Program for CANDU Reactor Core Design and Analysis", Proceedings of the 13th Pacific Basin Nuclear Conference, Shenzhen, China, Oct. 21-25, 2002.

- [2] B. Hanna, "CATHENA: A Thermalhydraulic Code for CANDU Analysis", J. Nuclear Engineering and Design, 180, p113-131.
- [3] C. Olive, L. Wilk, P. Sermer, D.H. Chung, S. Goodchild, M.K. O'Neill, R. Laidler, "Upgrades to the Simulation Of Reactor Operation (SORO) code for core-follow simulations of Ontario Power Generation and Bruce Power Reactors", IAEA TM on ASAM, 20071030-1102, KINS, Daejeon, Korea
- [4] G. Marleau, A. Hebert, and R. Roy, "A User Guide for DRAGON", Report IGE-174, Rev.5, École Polytechnique de Montréal , April 2000.
- [5] M. Dahmani, "Qualification and Development Plan for the T16MAC Version 1.0", AECL Report 153-113190-PLA-002, Rev. 0, 2007 November.
- [6] D. Altiparmakov, "New Capabilities of the Lattice Code WIMS-AECL", Proc. Int. Conf. on Reactor Physics, Nuclear Power: A Sustainable Resource, PHYSOR-2008, Interlaken, Switzerland, September 14-19, 2008.
- [7] T. Liang, W. Shen, E. Varin and K. Ho, "Improvement and Qualification of WIMS Utilities", 29th Annual CNS Conference, Toronto, June 1 - 4, 2008
- [8] Dai-Hai Chung, Hyung-Jin Kim, Sung-Min Kim and Hyeong-Taek Kim, "Effects of Structural Materials for RFSP-IST Modelling of Wolsong CANDU 6 Reactors on BP/CP Uncertainty Studies", 32nd Annual CNS Conference, Niagara Falls, ON, June 5 - 8, 2011
- [9] S. R. Kim and B. J. Moon, "CATHENA Multiple Average Channel Model", 59RF-03500-AR-041, Rev. 1, KOPEC, 2009.04.30.
- [10] R.D. McArthur and S.Z. Snell, "A Script for The Automated Coupling of Neutronics and Thermalhydraulics Codes for The Simulation of Fast Transients", Proceedings of the 21st Nuclear Simulation Symposium; Ottawa, Ontario, Toronto; Canadian Nuclear Society; 2000 Sep. 24-26.